

Article

Comparative Analysis of the Surface Urban Heat Island (SUHI) Effect Based on the Local Climate Zone (LCZ) Classification Scheme for Two Japanese Cities, Hiroshima, and Sapporo

Neshat Rahmani ¹ and Ayyoob Sharifi ^{2,*} 

¹ Graduate School of Advanced Science and Engineering, Hiroshima University, Hiroshima 739-8511, Japan; m221102@hiroshima-u.ac.jp

² The IDEC Institute, and Network for Education and Research on Peace and Sustainability (NERPS), Hiroshima University, Hiroshima 739-8529, Japan

* Correspondence: sharifi@hiroshima-u.ac.jp

Abstract: The Local Climate Zone (LCZ) classification system is used in this study to analyze the impacts of urban morphology on a surface urban heat island (SUHI). Our study involved a comparative analysis of SUHI effects in two Japanese cities, Sapporo and Hiroshima, between 2000 to 2022. We used geographical-information-system (GIS) mapping techniques to measure temporal LST changes using Landsat 7 and 8 images during the summer's hottest month (August) and classified the study area into LCZ classes using The World Urban Database and Access Portal Tools (WUDAPT) method with Google Earth Pro. The urban thermal field variance index (UTFVI) is used to examine each LCZ's thermal comfort level, and the SUHI heat spots (HS) in each LCZ classes are identified. The research findings indicate that the mean LST in Sapporo only experienced a 0.5 °C increase over the time, while the mean LST increased by 1.8 °C in Hiroshima City between 2000 and 2022. In 2000, open low-rise (LCZ 6) areas in Sapporo were the hottest, but by 2022, heavy industry (LCZ 10) became the hottest. In Hiroshima, compact mid-rise (LCZ 2) areas were the hottest in 2000, but by 2022, heavy-industry areas took the lead. The study found that LCZ 10, LCZ 8, LCZ E, and LCZ 3 areas in both Dfa and Cfa climate classifications had unfavorable UTFVI conditions. This was attributed to factors such as a high concentration of heat-absorbing materials, impervious surfaces, and limited green spaces. The majority of the SUHI HS and areas with the highest surface temperatures were situated near industrial zones and large low-rise urban forms in both cities. The study offers valuable insights into the potential long-term effects of various urban forms on the SUHI phenomenon.

Keywords: surface urban heat island (SUHI); local climate zones (LCZs); land surface temperature (LST); climate change adaptation; Sapporo; Hiroshima



Citation: Rahmani, N.; Sharifi, A. Comparative Analysis of the Surface Urban Heat Island (SUHI) Effect Based on the Local Climate Zone (LCZ) Classification Scheme for Two Japanese Cities, Hiroshima, and Sapporo. *Climate* **2023**, *11*, 142. <https://doi.org/10.3390/cli11070142>

Academic Editor: Nir Y. Krakauer

Received: 25 May 2023

Revised: 5 July 2023

Accepted: 6 July 2023

Published: 10 July 2023



Copyright: © 2023 by the authors. Licensee MDPI, Basel, Switzerland. This article is an open access article distributed under the terms and conditions of the Creative Commons Attribution (CC BY) license (<https://creativecommons.org/licenses/by/4.0/>).

1. Introduction

By 2050, the world's urban population is predicted to increase from 55% to 68% [1]. This means an additional 2.5 billion people living in cities [2]. This urbanization process alters the demographic, socioeconomic, and physical aspects of a landscape, resulting in different impacts on greenhouse gas (GHG) emissions based on the level of development of the countries involved [3].

The process of urbanization results in the creation of an urban heat island (UHI), where cities are hotter than the surrounding rural areas [4,5]. This phenomenon exacerbates the effects of climate change and raises the frequency and severity of heat waves, highlighting the importance of comprehending their combined impacts to adapt to climate change and mitigate health impacts [6,7]. Urban dwellers are at a higher risk of experiencing heat-related illnesses due to the UHI effect [8,9]. There are different categories of UHIs that can be classified based on their spatiotemporal characteristics and the mechanisms that cause them [4]. These include surface urban heat island SUHI, subsurface urban heat

islands (SUHI), canopy layer urban heat islands (CUHI), and boundary layer urban heat islands [10]. UHI studies have mainly focused on SUHI and CUHI [11]. LST detected by thermal infrared (TIR) sensors on satellites is commonly used to detect SUHI [12]. Landsat thermal imagery is the preferred dataset for SUHI studies due to its widespread availability and high spatial resolution, making it popular for SUHI analysis [13]. Most research on SUHI using Landsat data has focused on land use and land-cover classification as a means of categorizing the thermal environment and demonstrating how significant these factors are in influencing the intensity of SUHI [14]. Many research studies have embraced the concept that the intensity of SUHI is significantly influenced by urban expansion and the background climate [15]. Some studies utilized the concept of SUHI intensity by measuring the difference in LST between urban areas and the suburban regions surrounding them [16]. For instance, a study conducted by [17] examined the Urban Heat Island (UHI) phenomenon in Shanghai. The findings of the study indicate that the changes in UHI over time and space are attributed to the swift expansion and sprawl of the urban area, which may result in an escalation of the UHI effect.

Similar research conducted on the Quanzhou region of southeast China over a 20-year period revealed that the increase in the percentage of built-up land can lead to a significant rise in LST [18]. Another study revealed that the differences in the normalized difference vegetation index between urban and rural areas have a greater influence on the variation in minimum temperature differences in Delhi and Mumbai, India [19]. Also, a study of two Canadian urban area in 2019 showed that the primary cause of the UHI effect is the built-up urban land [20].

Several research studies have attempted to utilize the LCZ Classification Scheme to investigate the impact of diverse urban forms on the SUHI phenomenon [21]. This approach is favored because it enables straightforward comparisons of SUHI effects among distinct urban patterns [22]. The LCZs comprise various surface covers, structures, and materials that span from hundreds of meters to several kilometers in horizontal scale. They consist of 10 distinct building types and 7 different types of land cover [23]. These categories were established to offer a consistent and structured framework for the research and modelling of urban climates, as well as to facilitate the development of sustainable urban environments [24]. The LCZs have been employed to study the impacts of urbanization on local climates and to devise approaches for reducing the severity of the UHI effect [25]. The LCZ methodology considers various factors such as vegetation, surface cover, and building height that influence the severity of the SUHI effect [26]. Therefore, it provides a more comprehensive understanding of the UHI phenomenon [25]. An example of the practical applications of the LCZ methodology is a study conducted in Texas in 2020 founded that LCZs can be valuable for comparing the SUHI effect between cities and for investigating changes in SUHI over time [21]. Moreover, understanding the spatial distribution of LCZs can help in devising effective strategies for mitigating the SUHI phenomenon [21]. A study conducted in Beijing employed 100 m resolution LST data to examine the SUHI phenomenon in different LCZs and demonstrated that the distinct LCZs play a role in the development of the SUHI effect, and that there is a more significant disparity in SUHI intensity between compact and open buildings [27].

However, still there is limited research on SUHI considering the LCZ classification scheme in Japanese cities. A study conducted on an urban heat island in Imaiara, Nagano Prefecture, Japan during 2003, found that at night, areas near high and low buildings were warmer than those in the countryside [28]. The study on the LCZ classification of Sendai, which is a typical example of large cities in Japan, used the World Urban Database and Access Portal Tools (WUDAPT) Level 0 methodology. It addressed the limitations of the Level 0 method in accurately classifying LCZs, particularly in built-up areas, and proposed a pre-set recognition of classes and parameter analysis [29]. Another study utilized remote sensing data to examine the UHI effect in Hiroshima city; they evaluated various variables that define the urban context, including population, building density, and urban morphology. The results of their study indicated that the UHI effect increases

proportionally with higher values of canyon height-to-width ratio, building density, and land surface temperature [30].

Several studies have utilized LCZ extracted from the WUDAPT level 0 data [31]. For instance, Ignatius et al. employed the LCZ classification scheme based on the WUDAPT level 0 methodology to investigate the UHI effect in Hong Kong. Their findings proposed that the WUDAPT level 0 data can be utilized as input data for mesoscale weather and climate modelling in the absence of precise urban morphology data [32]. Another study generated LCZ maps for Guangzhou and Wuhan, China, using both the WUDAPT and advanced spaceborne thermal emission and reflection radiometer (ASTER) methods. Their study revealed that future applications of WUDAPT for high-density cities can combine both ASTER and Landsat data [18]. A study conducted in 2022 in China aimed to examine how LST reflects the UHI intensity. They created an LCZ map of the Yangtze River Delta (YRD) megaregion using the WUDAPT method and found that LST is in line with the LCZ classes in various cities in the YRD, with higher LST being observed in built-up LCZ classes [33].

The LCZ categorizes cities based on their urban forms. On the other hand, the Koppen climate classification system categorizes regions based on their temperature, precipitation, and vegetation patterns [34]. These two concepts are related in that the UHI effect can be more significant in certain climates. The Koppen–Geiger climate classification, which is commonly used, identifies five primary climate types: tropical, dry, temperate, continental, and polar. These classifications are based on factors such as temperature and precipitation patterns [35]. Specifically, in the case studies of this research, Sapporo city is categorized as Dfa, while Hiroshima city is categorized as Cfa [36]. The humid subtropical climate is a defining feature of the Cfa climate type, while the Dfa climate type is distinguished by a humid continental climate. These classifications have been frequently utilized in research to gain insights into the climate conditions and possible environmental hazards prevalent in these regions [37].

Despite numerous studies that have investigated the SUHI phenomenon using LCZ and Koppen climate classification schemes, there is still a significant research gap in the temporal comparative analysis of SUHIs and LCZs in cities with different climatic classes. Therefore, there is a need for further research in this area to better understand the potential impact of the LCZ on SUHIs in cities with different climatic conditions. The aim of our research was to analyze the impact of diverse urban configurations and climatic conditions on the magnitude of SUHI in two Japanese cities located in the northern and western regions of the country, which are classified as Cfa and Dfa, respectively. Although these cities share similar population, area, and density characteristics, their climates are distinct, and they were chosen to represent the climatic conditions of Japan from 2000 to 2022. We used a WUDAPT-based method to classify LCZs, and a GIS-based method to calculate LST. We sought to address the following questions:

How does the SUHI intensity associate with the LCZs in Hiroshima and Sapporo?

How does the UTFVI differ in each LCZ class?

Where are SUHI HSs in the selected cities and to which LCZs do they belong?

Aligned with these questions, the main goals of this paper can be summarized as follows: Firstly, to create a GIS-based method coupled with WUDAPT to generate LST and LCZ maps. Secondly, to examine the distribution and variation of surface temperature according to the specific climatic conditions of the cities, with a particular focus on using WUDAPT L0 data for assessing SUHI. Thirdly, to evaluate the UTFVI for each LCZ class to describe the thermal comfort and environmental conditions of each LCZ class. Finally, to identify the SUHI HS for UHI adaptation and mitigation in two cities and to provide a long-term comparison of SUHI using the LCZ scheme for the two cities while considering the impact of climate.

The study's workflow (Figure 1) involves a comprehensive approach to addressing the SUHI effect in two cities with different climatic conditions. To achieve this, the research developed a GIS-based method in conjunction with the WUDAPT method to produce

LST based on LCZs, analyzed the surface temperature variation and distribution over a 22-year period (2000–2022) according to the cities' specific climatic conditions, and identified the SUHI UTFVI level of each LCZ and their HSs for adaptation and mitigation to support sustainable urban planning. The study's findings can provide valuable insights for policymakers and urban planners in making informed decisions for sustainable urban development.

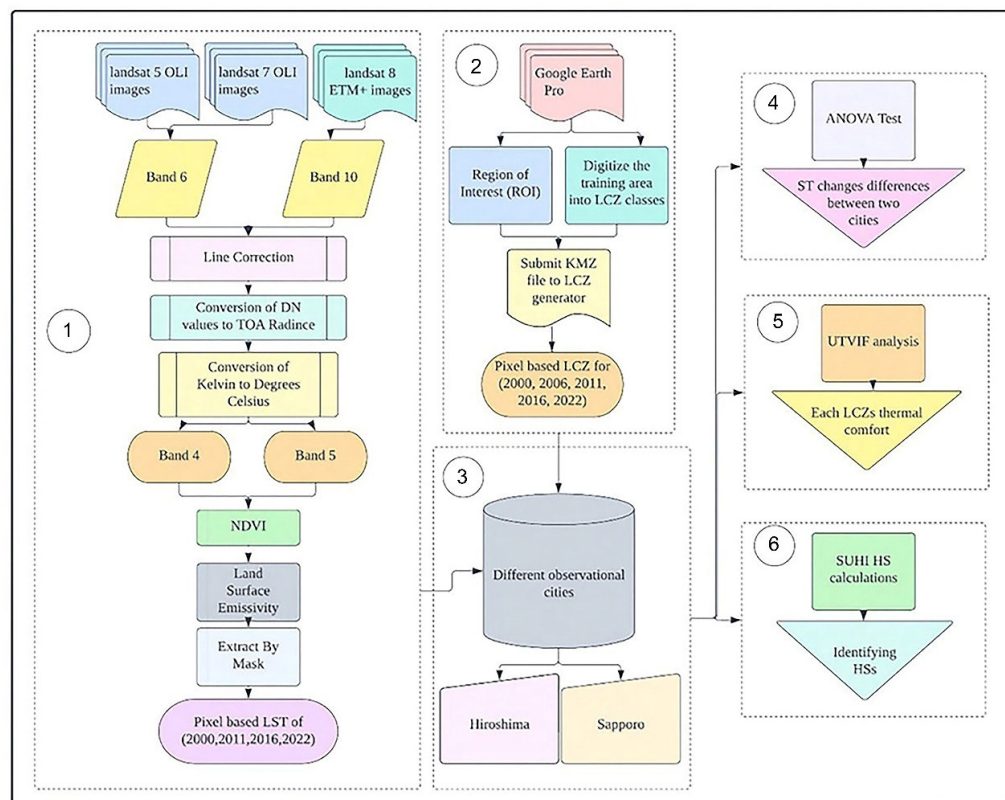


Figure 1. The workflow of the study.

2. Materials and Methods

2.1. Study Areas

2.1.1. Sapporo City

Location of the study areas is shown in Figure 2. Sapporo is a city with a population of 2,666,000 as of 2023 and a population density of 1746 people per km² [38]. It is situated at 43°04′0.01″ N and 141°20′60.00″ E. It is the biggest city in Hokkaido and the regional administrative, commercial, and cultural hub. The climate in Sapporo is classified as Dfa according to the Koppen and Geiger climate classification, with cold, snowy winters and hot, rainy summers. The annual rainfall in Sapporo is 1266 mm, and the average temperature is 6.2 °C. The city is one of the snowiest in the world because of the extremely low winter temperatures that can reach −15 °C. The summertime monsoon season can lead to bad weather, and there are many disturbances in the air during the spring and fall.

2.1.2. Hiroshima City

The city of Hiroshima, which is located at 34°23′60.00″ N and 132°26′60.00″ E, has 1,190,226 residents in 2023 [39]. This city has a population density of 1321 people per km². Like a large portion of the rest of Japan, Hiroshima experiences hot, humid summers and cool to mild winters. The city receives a lot of rain throughout the year, with June and July being the wettest months, and August being the warmest month of the year. According to the Koppen and Geiger climate classifications, the city has a Cfa climate with an average temperature of 14.3 °C and a total precipitation of 1601 mm.

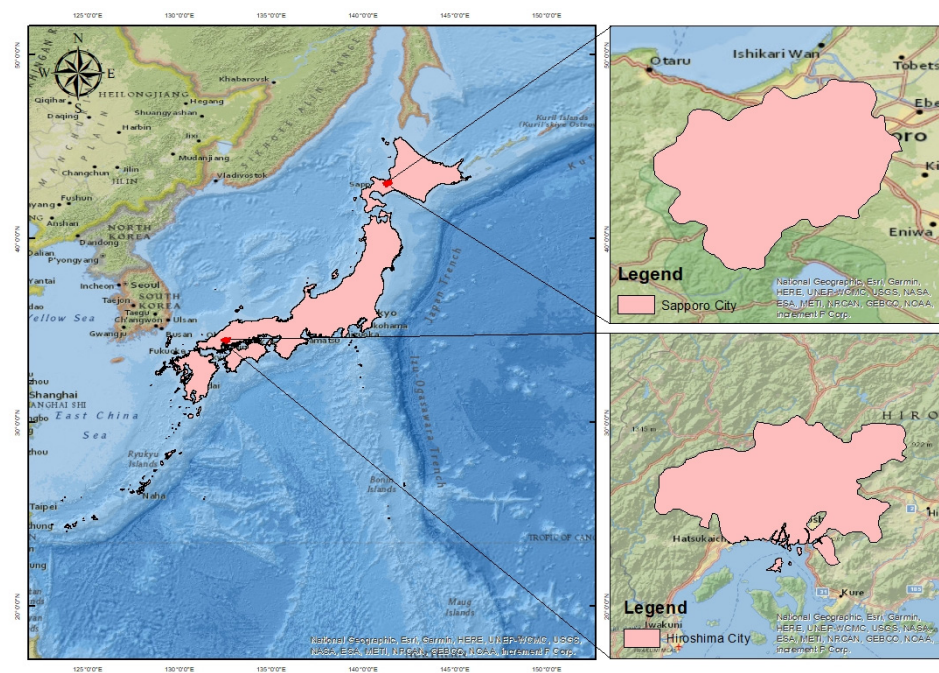


Figure 2. Location of the study area and the two cities boundary is according to (DIVA-GIS, free, simple and effective).

2.2. Data Collection

The study area’s LST data were obtained using Landsat 5 TM and 7 ETM+ and Landsat 8 OLI/TIRS sensors for the years 2000, 2006, 2011, 2016, and 2022 (Tables 1 and 2). In this study, we downloaded ten sets of thermal-infrared images captured by remote sensing with a 30-m spatial resolution and less than 20% cloud cover during August, the hottest month of the year, from <http://earthexplorer.usgs.gov>, 2 March 2023. These data were used to analyze the 5- to 6-year variation of LST and SUHI.

Table 1. Landsat dataset specification for Sapporo city.

Years	Landsat	Date	Time	Sun Elevation	Cloud Cover	Earth-Sun Distance (AU)
2000	5 ETM+	4 August 2000	12:58:05 p.m.	48.02616763	4.00	1.0084427
2006	7 ETM+	29 August 2006	01:09:27 p.m.	41.19074121	5.00	1.0018461
2011	8 OLI/TIRS	27 August 2011	01:13:15 p.m.	42.32630942	10.00	1.0024991
2016	8 OLI/TIRS	28 August 2016	01:19:50 p.m.	64.11945817	20.65	1.0166175
2022	8 OLI/TIRS	9 August 2022	01:20:14 p.m.	48.81951489	0.01	1.0073422

Table 2. Landsat dataset specification for Hiroshima city.

Years	Landsat	Date	Time	Sun Elevation	Cloud Cover	Earth-Sun Distance (AU)
2000	5 ETM+	14 September 2000	12:39:39 p.m.	38.69539399	1.00	1.0057351
2006	7 ETM+	24 August 2006	01:36:46 p.m.	57.59674555	5.00	1.0110896
2011	8 OLI/TIRS	7 August 2011	01:40:27 p.m.	54.86613552	3.00	1.0078970
2016	8 OLI/TIRS	28 August 2016	01:19:50 p.m.	64.11945817	23.99	1.0166175
2022	8 OLI/TIRS	27 August 2022	01:47:30 p.m.	64.63900693	16.99	1.0156254

2.3. LST Calculations

For our research, we utilized satellite images from Landsat 7 and 8, which were obtained from the USGS website and freely accessible for research purposes. These images were packaged with 12 band images. We focused on using thermal bands 4, 5, and 6 for the years 2000 and 2006, and bands 4, 5, and 10 for the years 2016 and 2022. By employing a GIS-based technique, we generated LST maps with a resolution of 30×30 m. These maps allowed us to analyze the Spatiotemporal Urban Heat Island (SUHI) effect and its changes over the study area during specific years [40]. The calculation procedure considered various factors, including the Normalized Difference Vegetation Index (NDVI), Brightness Temperature (BT), and Land Surface Emissivity (LSE), as well as the thermal bands of Landsat 7 and Landsat 8 satellite images [18].

Using GIS and information from Landsat 5 and 7 satellites, the following equations were employed to calculate LST for the years 2000 and 2011:

The USGS standard Equation (1) was used to convert the digital numbers (DNs) of the thermal bands into spectral radiance.

$$L\gamma = \frac{LMAX\gamma - LMIN\gamma}{QCALMAX - QCALMIN} \times (QCAL - QCALMIN) + LMIN\gamma \tag{1}$$

The metadata file (MTL) provided all the values used in the computation, including $Lmax\gamma$ and $Lmin\gamma$, which represent the spectral radiance scaled to $QCALmax$ and $QCALmin$, respectively, measured in $(Watts/(m^2 \times sr \times \mu m))$. $QCALmax$ and $QCALmin$ are the maximum and minimum quantized calibrated pixel values, respectively, which correspond to $Lmax\gamma$ and $Lmin\gamma$, while $QCAL$ denotes the quantized calibrated pixel value in DN. The formula calculates the spectral radiance, $L\gamma$.

To convert radiance to BT, Equation (2) was utilized.

$$T = \frac{K2}{\frac{\ln(K1)}{L\gamma} + 1} \tag{2}$$

The formula used to convert radiance to BT involved the effective at-satellite temperature (T) in Kelvin, along with calibration constants K1 and K2, and spectral radiance ($L\gamma$) measured in $(Watts/(m^2 \times sr \times \mu m))$. For the Landsat-7 image, VCID 1 and VCID 2 in Band 6 have K1 constants of 666.09 and K2 constants of 1282.71.

To convert Kelvin to degrees Celsius, the formula (3) was applied.

$$C = (K) (-273.15) \tag{3}$$

The process of computing LST for the years 2016 and 2022 using GIS was carried out by employing certain mathematical expressions. These expressions were applied to data gathered from Landsat 8 and 9 satellites.

The conversion of the thermal bands' DN to top-of-atmosphere (TOA) radiance was accomplished by applying Formula (4).

$$L\gamma = ML * Qcal + AL - Oi \tag{4}$$

The formula used to convert DN to TOA radiance involved several parameters. These parameters included the TOA spectral radiance ($L\gamma$) measured in $(Watts/(m^2 \times sr \times \mu m))$, the band-specific multiplicative (ML) and additive (AL) rescaling factors obtained from the metadata file, the quantized and calibrated standard product pixel values (Qcal), and the correction value (Oi) for Band 10.

Formula (5) was employed to transform the radiance image to BT for the thermal band.

$$K \text{ to Celsius degrees } BT = \frac{K2}{\ln\left\{\left[\left(\frac{K1}{L\gamma}\right) + 1\right]\right\}} - 273.15 \tag{5}$$

To convert TOA spectral radiance to the TOA and BT, Equation (5) was applied. TOA spectral radiance ($L\gamma$) was measured in ($\text{Watts}/(\text{m}^2 \times \text{sr} \times \mu\text{m})$), band-specific thermal conversion constants (K1 and K2) obtained from metadata, and the absolute zero (approximately -273.15 °C). In this study, Band 10 for the Landsat-8 image used K1 and K2 constants of 774.8853 and 1321.0789, respectively.

Equation (6) utilizes the RED/NIR band ratio to determine the NDVI value.

$$NDVI = \frac{NIR - RED}{NIR + RED} \quad (6)$$

In Equation (6), the NDVI value is derived by using the DN values from the RED band and near-infrared band.

Equation (7) was utilized to determine the proportion of vegetation (Pv):

$$Pv = \left[\frac{NDVI - NDVImin}{NDVImax - NDVImin} \right] \quad (7)$$

where, in Equation (7), the Pv is determined based on the DN values from the NDVI image, maximum DN values from the NDVI image ($NDVImax$), and minimum DN values from the NDVI image ($NDVImin$).

Equation (8) is used for the estimation of emissivity (ϵ) in surface calculations.

$$\epsilon = 0.004 \times Pv + 0.986 \quad (8)$$

In the given equation, the land surface ϵ is estimated by incorporating the proportion of Pv and a correction value of 0.986.

The LST was calculated using Equation (9), which involves using the emissivity-corrected BT.

$$Ts = \frac{BT}{\left\{ \left[1 + \left(\frac{\gamma BT}{\rho} \right) \ln \epsilon \gamma \right] \right\}} \quad (9)$$

Equation (9) is used to calculate the LST in Celsius by taking into account the at-sensor BT and the emissivity ($\epsilon\gamma$) at the average wavelength (γ) of band 10.

2.4. The Analysis of Variance (ANOVA)

The ANOVA test is a statistical tool used to determine if there is a significant difference between the means of two or more groups [41]. The ANOVA test formula involved several steps that can be broken down as follows:

First, calculations of the total sum of squares (SST) by summing the squared differences between each data point and the overall mean. The SST represents the total variation in the data:

$$SST = \sum (X - X^-)^2 \quad (10)$$

where X is each data point, and X^- is the overall mean of all data points.

Next, the calculation of the sum of squares between groups (SSB) was performed by summing the squared differences between each group mean and the overall mean, weighted by the number of observations in each group. The SSB represents the variation between the group means.

$$SSB = \sum ni(X^-i - X^-)^2 \quad (11)$$

where ni is the number of observations in each group, X^-i is the mean of each group, and X^- is the overall mean.

Then, calculations of the sum of squares within groups (SSW) by summing the squared differences between each data point and its respective group mean. The SSW represents the variation within each group.

$$SSW = \sum \sum (Xij - X^-i)^2 \quad (12)$$

where X_{ij} is each data point in each group, and \bar{X}_i is the mean of each group.

After that, calculations of the degrees of freedom for the between-group (dfB), within-group (dfW), and total (dfT) sources of variation.

$$dfB = k - 1 \quad (13)$$

where k is the number of groups.

$$dfW = N - k \quad (14)$$

where N is the total number of observations.

$$dfT = N - 1 \quad (15)$$

where dfT is used to calculate the mean square values (MSB and MSW) by dividing the sum of squares by the corresponding degrees of freedom.

$$MSB = SSB/dfB \quad (16)$$

$$MSW = SSW/dfW \quad (17)$$

Calculation of the F-value was performed by dividing the mean square value for between-group variation (MSB) by the mean square value for within-group variation (MSW).

$$F = MSB/MSW \quad (18)$$

Next, find the p -value associated with the F-value using an F-distribution table or statistical software.

$$p\text{-value} = P(F \geq F_{calc}) = 1 - P(F < F_{calc}) \quad (19)$$

By using ANOVA, it is possible to compare the statistical difference between the mean surface temperature values of the two cities and determine if the difference is significant or due to chance.

2.5. Local Climate Zone Classification

In this study, the land surface characteristics of the study area were classified into 10 different built-up zone types and seven different land-cover area types (Figure 3) using the Stewart and Oke's LCZ classification scheme [25]. Classification of the LCZ was conducted using a tool called WUDAPT.

WUDAPT is a powerful tool for LCZ classification because it utilizes a combination of remote sensing data, machine learning algorithms, and human expertise to classify urban areas based on their surface cover characteristics. This approach allows for a more objective and consistent method of classification compared to traditional methods, which rely solely on a subjective visual interpretation of aerial or satellite imagery. This tool is a community-based project that classifies urban fabric according to climate properties, utilizing data available on a global scale, and it calculates LCZs with resolutions ranging from 300 m to 10 km [42].

2.6. Method for Measurement of SUHI

The LCZ classification and comparison of LST between LCZ classes are used to measure the SUHI. Understanding the factors influencing the UHI effect can be accomplished by calculating the SUHI using the LCZ classification and comparing LST between LCZ classes. The LST difference between the given LCZ type (LST_{LCZx}) and LCZ D is the formula for calculating the SUHI of a particular LCZ type (SUHI_{LCZx}) (LST_{LCZD}). This can help identify areas with different thermal characteristics and provide insights into the factors that contribute to the SUHI effect [22].

Equation (10) involves comparing the statistical data of the surface temperature (T_s) in one LCZ class with those in another LCZ class.

$$SUHI_{LCZx} = LST_{LCZx} - LST_{LCZD} \tag{20}$$

Equation (20) calculates the SUHI of an LCZ X type, which is the difference between its mean LST (LST_{LCZx}) and the mean LST of a reference LCZ D (such as grassland, farmland, or urban park) represented by LST_{LCZD} . The $SUHI_{LCZx}$ indicates the SUHI value of the LCZ X type [43].

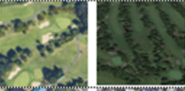
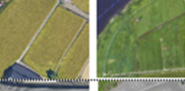
Built up type	Hiroshima Sapporo	Land cover type	Hiroshima Sapporo
LCZ1: Compact high-rise		LCZA: Dense trees	
LCZ2: Compact mid-rise		LCZB: Scattered trees	
LCZ3: Compact low-rise		LCZC: Bush, Scrub	
LCZ4: Open high-rise		LCZD: Low plants	
LCZ5: Open mid-rise		LCZE: Bare rock and paved	
LCZ6: Open low-rise		LCZF: Bare soil and sand	
LCZ7: Lightweight low-rise	Not existed	LCZG: Water	
LCZ8: Large low-rise			
LCZ9: Sparsely built			
LCZ10: Heavy industry			

Figure 3. Local climate zone classification scheme and samples from the selected cities (Stewart and Oke, 2012 [35]).

2.7. The Urban Thermal Field Variance Index (UTFVI)

Calculating the UTFVI for every LCZ class is important because it provides a way to evaluate the thermal environment and quality of life within different areas of the city. By measuring the variance in surface temperature compared to the mean temperature of the area (T_{mean}), the UTFVI can indicate which areas are more prone to extreme temperatures and can help identify potential areas for intervention and improvement. Equation (11) is used to calculate the UTFVI, an important indicator of the environmental conditions and quality of urban health. The formula divides the difference between the temperature of a location (T_s) and the mean temperature (T_{mean}) by the mean temperature. The UTFVI is widely used to guide urban-planning and -design decisions aimed at improving the well-being of city residents, as demonstrated by [44].

The UTFVI was calculated using Equation (21), as described by [45]:

$$UTFVI = \frac{T_s - T_{mean}}{T_{mean}} \tag{21}$$

where T_s is the LST, T_{mean} is the mean LST, and UTFVI is the output. The UTFVI was assessed and classified into six distinct conditions to provide a comprehensive understanding of thermal comfort levels. These conditions were categorized as follows [46]:

1. Excellent Condition (EC): This category represents thermal comfort levels with a range below zero (<0), indicating an exceptionally comfortable environment.
2. Good Condition (GC): The thermal comfort falls within the range of 0 to 0.005, indicating a highly favorable and comfortable urban setting.
3. Normal Condition (NC): In this category, the UTFVI ranges from 0.010 to 0.015, representing a typical or average level of thermal comfort.
4. Bad Condition (BC): The thermal comfort level falls within the range of 0.015 to 0.020, indicating a less favorable and potentially uncomfortable urban environment.
5. Worse Condition (WC): This category represents thermal comfort conditions above 0.020, signifying a significantly unfavorable and uncomfortable urban setting.

This classification system can help urban planners and policymakers identify areas with poor thermal comfort conditions and prioritize interventions to improve them. Additionally, it can aid in understanding the relationship between LCZs and thermal comfort in urban areas.

2.8. Uncertainty Calculations

To evaluate the uncertainties associated with our LST calculations, we performed an analysis to validate the accuracy of our measured LST values. We employed the widely available MODIS LST maps, which provide a resolution of 1 km, as a reference dataset for comparison. This approach allowed us to quantify the consistency between our measurements and a trusted remote sensing dataset, thus enhancing the reliability of our findings [47].

The average error in the surface temperature algorithm was calculated by comparing the measured surface temperatures with the corresponding MODIS LST data. The formula used to determine the average error is as follows:

1. Individual Measurement Error Calculation: For each measurement, we computed the error by subtracting the reference surface temperature (or ground truth temperature) from the corresponding measured temperature. This can be expressed as:

$$\text{Error} = \text{Measured LST} - \text{Reference LST}$$

2. Summation of Individual Errors: We aggregated the individual errors by summing them up for all the measurements, leading to the calculation of the sum of errors:

$$\text{Sum of Errors} = \text{Error}_1 + \text{Error}_2 + \text{Error}_3 + \dots + \text{Error}_N$$

3. Calculation of Average Error: To obtain the average error, we divided the sum of errors by the total number of measurements (N). This formula provides the average difference between the measured surface temperatures and the reference temperatures across all the measurements:

$$\text{Average Error} = \text{Sum of Errors}/N$$

By employing this formula, we quantified the average deviation of our LST measurements from the reference values. This metric serves as an indicator of the overall bias or deviation of the surface temperature algorithm utilized in our study.

3. Results

3.1. LCZ Maps

To begin with, regions of interest (ROI) were established based on the individual cities' boundaries, and training samples for all LCZ types were selected for Hiroshima and Sapporo in the years 2000 and 2022. LCZ classification maps were created, and the

WUDAPT machine learning model was used to map LCZs in the study area, accurately classifying the LCZs for both cities (Figure 4). To improve accuracy and reduce errors, the study only considered homogenous LCZs with a diameter of approximately 1 km. However, our LCZ mapping scheme failed to identify LCZ 7, a unique category not commonly found in urban areas, and therefore excluded it from subsequent analysis. Overall, the LCZ maps for both metropolitan areas showed a similar pattern, with “built-up” LCZ types typically surrounded by “natural” LCZ types A-G. The central urbanized area of both cities is primarily populated with “built-up” LCZ types, while LCZ A dense trees predominate the surrounding rural areas. Regarding “built-up” LCZ types, there is a tendency for the majority of the urbanized area to be classified as “compact” LCZ types (e.g., LCZ 1 compact high-rise, LCZ 2 compact mid-rise, LCZ 3 compact low-rise).

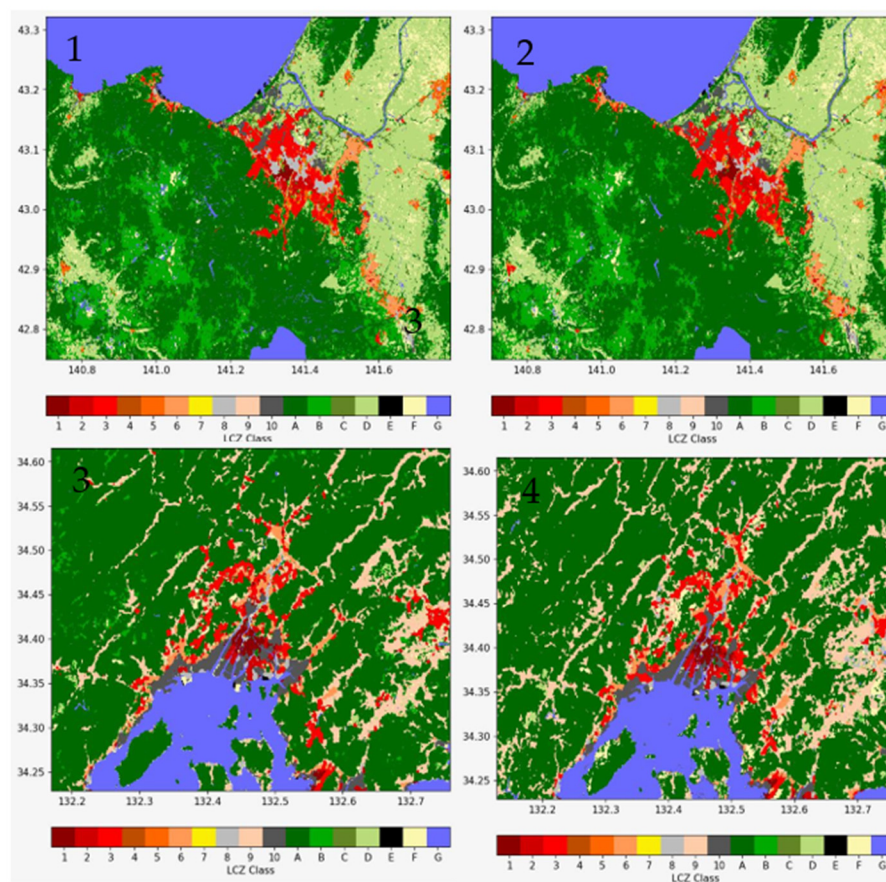


Figure 4. (1) LCZ classification map of Sapporo city (2000), (2) LCZ classification map of Sapporo city (2022), (3) LCZ classification map of Hiroshima city (2000), and (4) LCZ classification map of Hiroshima City (2022).

3.2. LST and LCZ Changes over Time

We examined the changes in LST in Sapporo City over the past two decades (from 2000 to 2022) to understand the spatial variation of LST and the UHI phenomenon. The results indicated that Sapporo City had only experienced a 0.5 °C increase in LST during this time frame, suggesting that the urban heat island effect in the city has remained relatively stable over the last two decades.

On the other hand, we found that there was a considerable increase of 1.8 °C in LST in Hiroshima City over the past two decades, based on the analysis of spatial variation of LST over time from 2000 to 2022. This suggests that the urban heat island effect in Hiroshima has considerably increased over the past twenty years, which may have important implications for the city’s residents and environment. Additionally, to investigate the mean surface temperature differences between the groups of Sapporo and Hiroshima, we conducted a

one-way analysis of variance (ANOVA) test. This statistical test allowed us to determine if there were any significant variations in the mean surface temperatures between the two locations. By comparing the temperature data collected from both Sapporo and Hiroshima, we were able to analyze the overall variability and ascertain whether any observed differences were statistically significant.

Table 3 shows that the sum of squares for the factor “Sapporo” is 7.674 with 1 degree of freedom, and the MSS for this factor is 7.674. The MSS was calculated by dividing the SS by the degrees of freedom. Similarly, the sum of squares for the factor “Hiroshima” was 2.170 with 8 degrees of freedom, and the MSS for this factor was 0.271. The F-value was calculated by dividing the MSS between groups (Sapporo and Hiroshima) by the MSS within groups. In this case, the F-value is 28.29, which indicates that there is a significant difference between the means of the two groups. The *p*-value is also very small (0.000712), which is less than the significance level of 0.05, suggesting strong evidence against the null hypothesis of no difference between the means. *p*-value = 0.000712 ***.

Table 3. ANOVA test results of LST mean over the time in Sapporo and Hiroshima cities.

Factor	Sum Square (SS)	Degree of Freedom (df)	Mean Sum Square (MSS = SS/df)	F (MSSbetween/MSSwithin)
Sapporo	7.674	1	7.674	28.29
Hiroshima	2.170	8	0.271	
Sum	9.844	9		

The total variance in the data is decomposed into two components: variance between groups (also known as “treatment variance”) and variance within groups (also known as “error variance”). The between-group variance represents the variation in the data that is due to differences between the groups or treatments being compared, while the within-group variance represents the variation that is due to individual differences within each group. Therefore, based on the results, we can conclude that there is a significant difference in the means of the two groups, and this difference is not likely due to chance alone.

The LST spatial patterns of SUHI indicate that the selected cities exhibited a noticeable change in SUHI effect between 2000 and 2022 (Figures 5 and 6). The study found that in 2000, the areas in Sapporo that were most sensitive to high temperatures were LCZ 6 (open low-rise), LCZ 2 (compact mid-rise), and LCZ 3 (compact low-rise), but this changed over time, with surface temperatures shifting towards larger buildings and industrial zones. By 2022, LCZ 10 (heavy industry), LCZ 8 (large low-rise), and LCZ 3 (compact low-rise) were the most sensitive to high temperatures. Generally, areas with a high concentration of buildings had a higher LST. However, in urban areas where buildings were spaced apart, like in LCZ 9, LST was lower. LST was higher near larger buildings in LCZ 10 and 8, but it was relatively low in the areas where there was more shade from taller buildings. Green areas had lower LST, and the surface temperature was even lower if the green areas were densely formed.

The analysis of Hiroshima found that in 2000, the LCZs most sensitive to high temperatures were LCZ 2 (compact mid-rise), LCZ 10 (heavy industry), and LCZ E (bare rock and paved) (Figure 7). The areas with high surface temperatures were still predominantly large buildings and heavy-concrete areas. In 2022, the highest LST was found in LCZ 10, LCZ E, and LCZ 8 (heavy industry, bare rock and paved and large low-rise). LST was generally higher in areas with more buildings, but even in urban areas where buildings were spaced apart, like in LCZ 9, LST was low. LST was higher near large buildings when examining LCZ 10 and 8, but relatively low in areas with high-rise buildings due to shade from taller buildings. All green areas and water bodies had lower surface temperatures, and even within one area, surface temperatures were lower when there were more green areas. In conclusion, the SUHI effect in Hiroshima was mostly associated with the presence of large buildings with low heights.

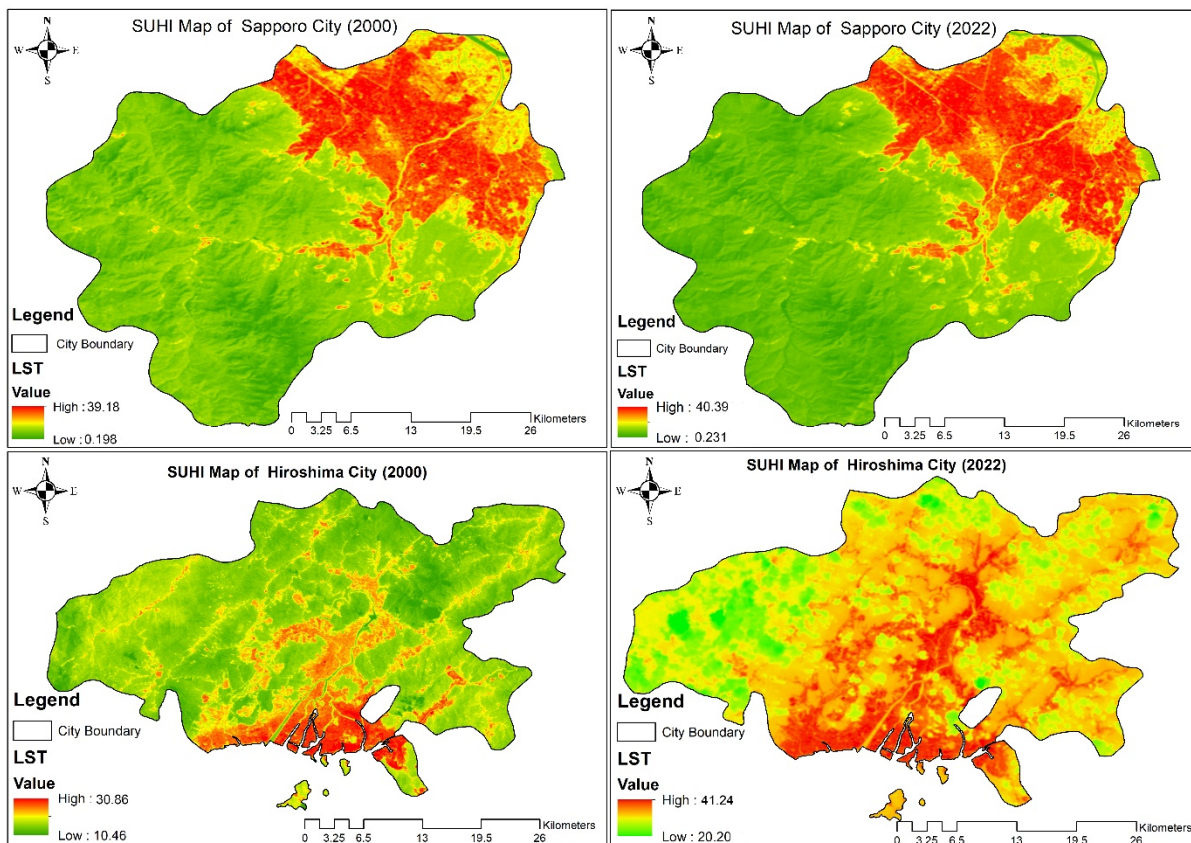


Figure 5. SUHI map of Sapporo and Hiroshima City from 2000 to 2022.

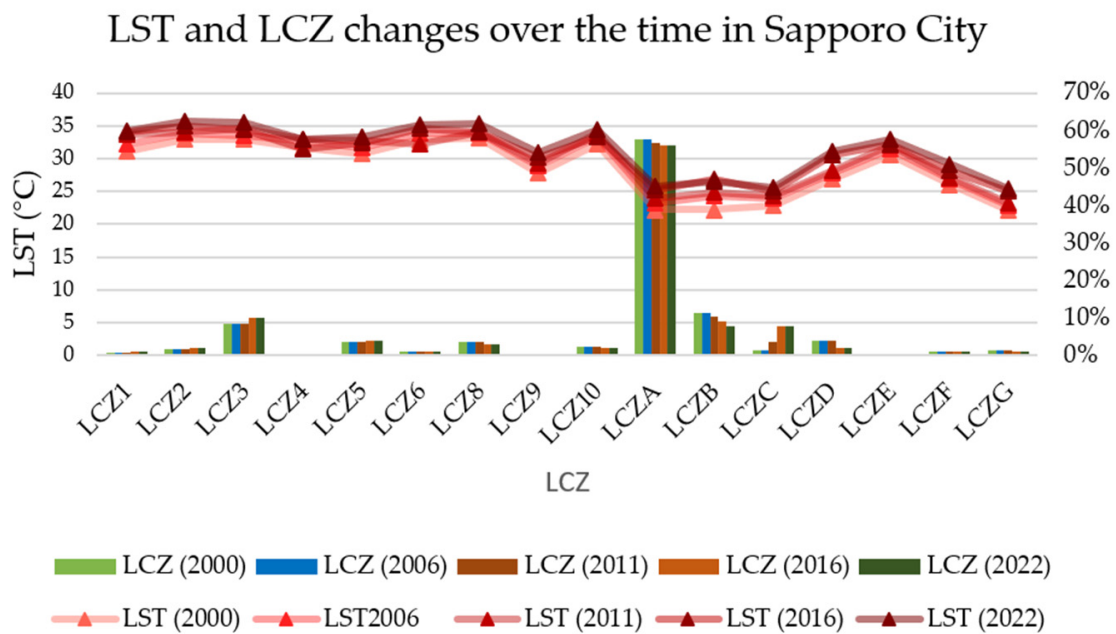


Figure 6. LST changes based on LCZ classification over the time in Sapporo city.

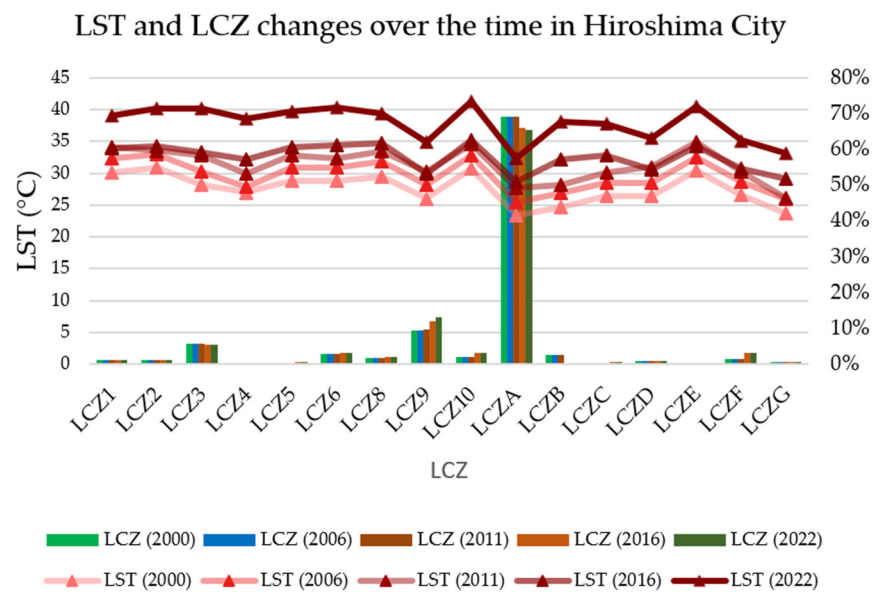


Figure 7. Changes based on LCZ classification over the time in Hiroshima city.

The spatial distribution of LST in each class of LCZs revealed different thermal characteristics among the zones. Although there were spatial differences in absolute LST values and LCZ variation between the two cities, the distribution of LST patterns for LCZs were generally consistent over time. This indicates that LCZs can be a valuable tool for characterizing urban thermal environments and identifying areas that are more susceptible to heat stress, regardless of their location within a city.

3.3. SUHI Distribution Variation over the Time

The spatial distribution of LST in individual LCZ classes over time in Sapporo and Hiroshima as shown in Figure 5 indicated different thermal characteristics among LCZs. In Sapporo city, LCZ 6 (open low-rise) had the highest LST with 39.18 °C in 2000, followed by LCZ 2 (compact high-rise) and LCZ 3 (compact low-rise). However, the surface temperature has shifted to other classes over the past two decades. In 2022, LCZ 10 (heavy industry) had the highest LST with 40.09 °C, followed by LCZ 8 (large low-rise) and LCZ 3 (compact low-rise). Recent studies have shown that urbanization and climate change have caused the surface temperature to shift towards higher LCZ classes [48], in line with that higher LST values observed in other classes in Sapporo city.

In Hiroshima City, LCZ 2 (compact mid-rise) had the highest LST in 2000 with 30.86 °C, followed by LCZ 10 (heavy industry) and LCZ E (bare rock and paved). However, the surface temperature has not shifted to other LCZ classes over the past 20 years. LCZ 10 and LCZ E still had the highest LST in 2022 with 41.24 °C and 40.52 °C, respectively, followed by LCZ 3 (compact low-rise) with 40.26 °C LST.

The comparison of the MODIS-driven LST values with the LST values generated by GIS using Landsat images reveals relatively small differences. In the case of Sapporo, the MODIS-driven LST shows a deviation of 0.13, while for Hiroshima, the deviation is 0.71. These relatively small differences indicate a low level of error and uncertainty in the LST calculations for both cities.

Based on these results, it can be concluded that the LST values derived from GIS using Landsat images are reliable. The minimal deviation between the MODIS-driven LST and the GIS-generated LST suggests that the algorithm employed in the surface temperature calculations exhibits a high level of accuracy.

3.4. SUHI Intensity Maps

Through the utilization of GIS tools, the SUHI intensity was assessed for each LCZ by conducting an analysis of LST data. This intensity metric characterizes the extent of

temperature variation between urbanized regions categorized as LCZ 1-10 and vegetated areas denoted as LCZ A-F. The evaluation involved the computation of the temperature disparity by subtracting the average LST value of the LCZ built-up areas from the average LST value of the vegetation areas.

Remarkably, Sapporo stood out with the highest SUHI intensity value observed in LCZ 10, measuring 0.25 (Figure 8). Following closely were values of 0.23 in LCZ 8 and 0.22 in LCZ E, indicative of a moderate level of the SUHI phenomenon within the city. Conversely, Hiroshima exhibited a notably higher SUHI intensity value, with LCZ 10 displaying a value of 0.9. This was accompanied by values of 0.7 in LCZ E and 0.52 in LCZ 3, suggesting a more pronounced and significant manifestation of the SUHI effect within the urban landscape of the city.

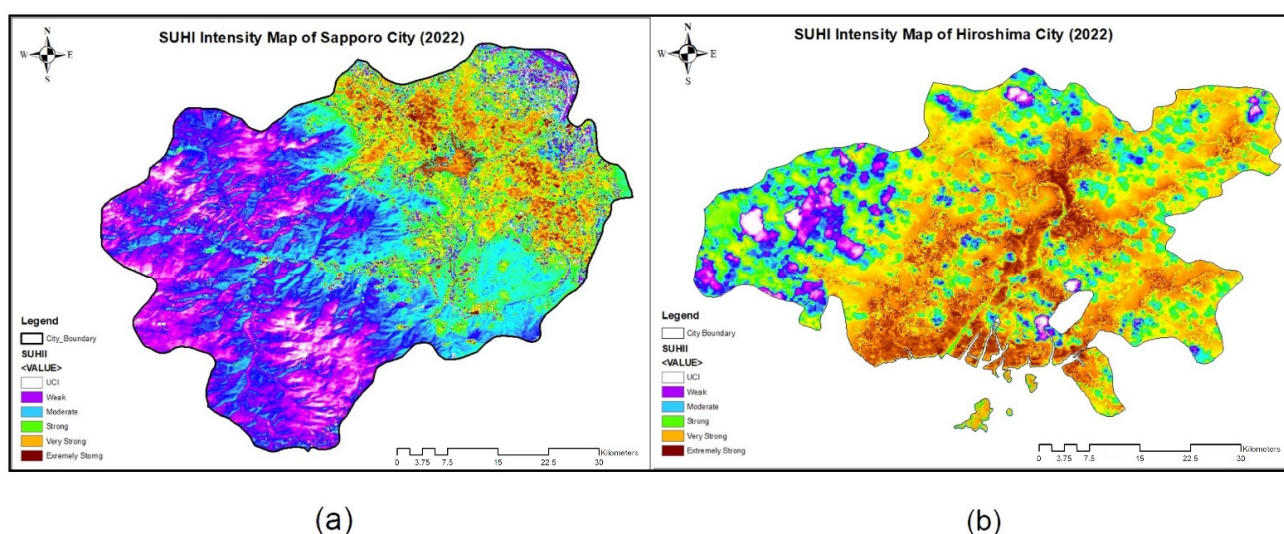


Figure 8. (a) SUHI distribution in every LCZ class for Sapporo city, (b) SUHI distribution in every LCZ class for Hiroshima city.

The overall SUHI intensity was observed to be low in Sapporo and relatively high in Hiroshima. The high SUHI intensity in both cities was observed in LCZ 3 (compact low-rise), LCZ 8 (large low-rise), LCZ 10 (heavy industry), and LCZ E (rock and paved), while LCZ A (dense trees), LCZ B (scattered trees), LCZ C (low plants), and LCZ 9 (sparsely built) showed the lowest SUHI intensity.

3.5. UTFVI Maps

To provide a clear overview of the environmental situation and thermal comfort in the two case-study cities, UTFVI maps were created from LST images for August 2022 and divided into 17 LCZ classes to identify areas with the highest temperatures and poorest thermal comfort conditions (Figure 9).

The UTFVI encompasses the following classes: excellent (EC), good (GC), normal (NC), bad (BC), and worst (WC). The excellent class signifies the highest level of UTFVI, indicating a highly favorable condition in terms of surface temperature. The “good” class represents a relatively favorable condition, while the “normal” class denotes a moderate level of UTFVI. The bad class indicates a higher level of vulnerability, suggesting a suboptimal condition. Finally, the worst class represents the highest level of UTFVI, indicating the most unfavorable condition in terms of surface temperature.

In Sapporo city, more than half of the study area had an excellent UTFVI ranking, indicating excellent thermal comfort for quality of life. The bad and worse UTFVI levels covered less than 10% of the area each. The worst category, which included horizontally expanded areas such as large buildings with concrete surfaces and metal roofs, had the poorest thermal comfort. In contrast, the majority of the study area in Hiroshima City had poor or atrocious thermal comfort, indicating poor thermal comfort for quality of life. More

than 20% of the city was covered by the bad condition (BC) UTFVI ranking. The worst category of the study area, which included large buildings with concrete surfaces and metal roofs, also had the worst thermal comfort.

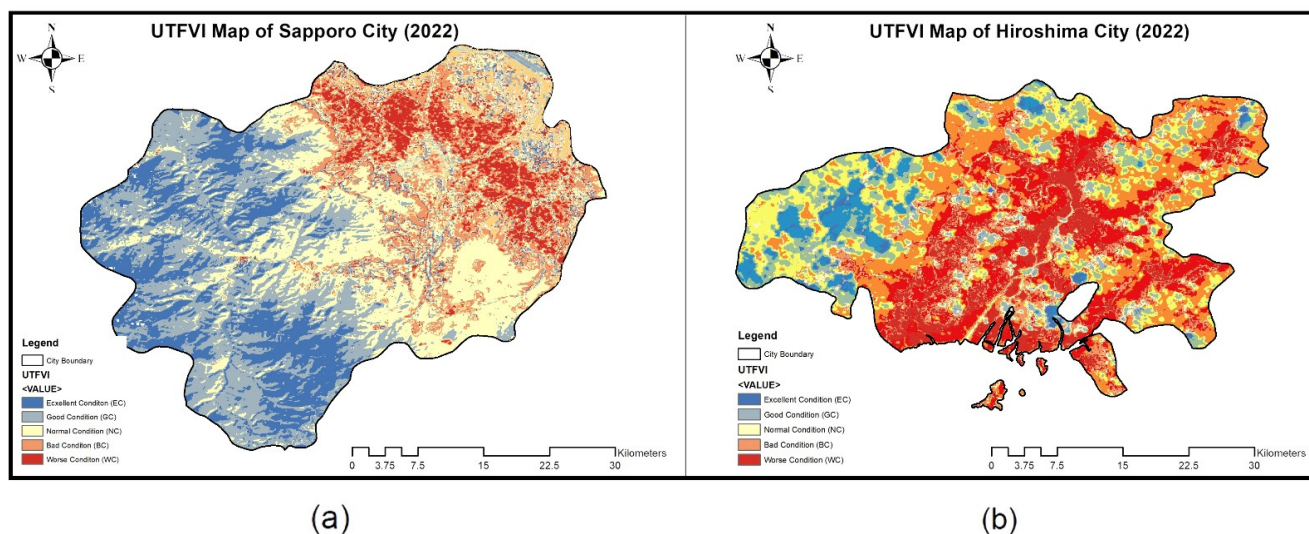


Figure 9. (a) UTFVI map of Sapporo (b) UTFVI map of Hiroshima city for 2022.

3.6. Relationship between UTFVI and LST in Different LCZ Classes

The UTFVI was used to assess the degree of thermal comfort in every LCZ area, with lower values indicating a more favorable or less severe SUHI. The findings reveal that the UTFVI values for LCZ8 in Sapporo city vary from -0.101 to 0.030 . Lower values within this range indicate a milder SUHI effect in those specific areas. Likewise, the LCZA values span from -0.015 to 0.010 , further indicating a relatively low level of the SUHI effect throughout the city. Overall, these results suggest that the SUHI effect in Sapporo city is relatively low, particularly in areas categorized as LCZ8.

For Hiroshima, the results indicate that the worst UTFVI value was in LCZ10, with values ranging from -0.366 to 0.048 . The best UTFVI value was found for LCZA, with values ranging from -0.033 to 0.012 , suggesting that areas categorized as LCZA have a lower level of the SUHI effect. Overall, the results suggest that the severity of the SUHI effect in Hiroshima varies depending on the land cover characteristics of each area. Areas with more urbanized land cover (LCZ10) tend to have a worse thermal field evaluation, while areas with more natural land cover (LCZA) tend to have a better evaluation.

3.7. SUHI Hotspots (HS)

The SUHI HSs over the study area were delineated from the SUHI map of two cities. The study identified the hotspots of the SUHI effect in two cities by analyzing the SUHI map, which took into account different types of land cover. Specifically, the study created maps of the HS where temperatures were higher than 40 degrees Celsius for Sapporo and 42 degrees Celsius for Hiroshima city. These high temperatures can have negative impacts on human health and lead to increased energy consumption for cooling, making it important to identify and manage these HS for the sake of urban planning and sustainable development.

The study's combined findings indicate that the hotspots of the SUHI effect in Sapporo are mainly located in areas classified as LCZ 3 (compact low-rise), LCZ 8 (large low-rise), and LCZ 10 (heavy industry), which experience the highest summertime surface temperatures (Figure 10). This information is valuable to urban planners and policymakers who can utilize it to develop effective strategies to mitigate the impacts of SUHI in Sapporo, particularly in these HS areas. Overall, the results of the study can be used to inform urban planning and policy decisions to reduce the impact of SUHI in Sapporo, particularly in hotspot areas classified as LCZ 3, LCZ 8, and LCZ 10.

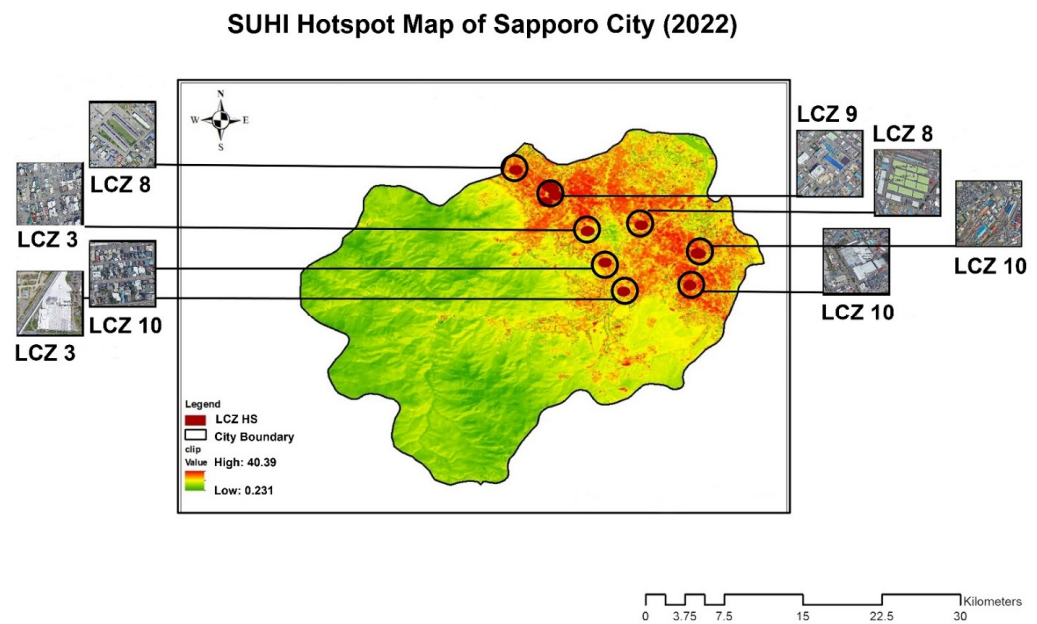


Figure 10. SUHI HS map of Sapporo city for 2022.

According to the study’s findings, the hotspots of the SUHI effect in Hiroshima (Figure 11) are concentrated in areas categorized as LCZ 2 (compact mid-rise), LCZ 8 (large low-rise), and LCZ 10 (heavy industry), which experience the highest summertime surface temperatures. Overall, the results of the study are important for urban planners and policymakers to consider when developing and implementing strategies to address the impact of SUHI in Hiroshima, particularly in areas categorized as LCZ 2, LCZ 8, and LCZ 10.

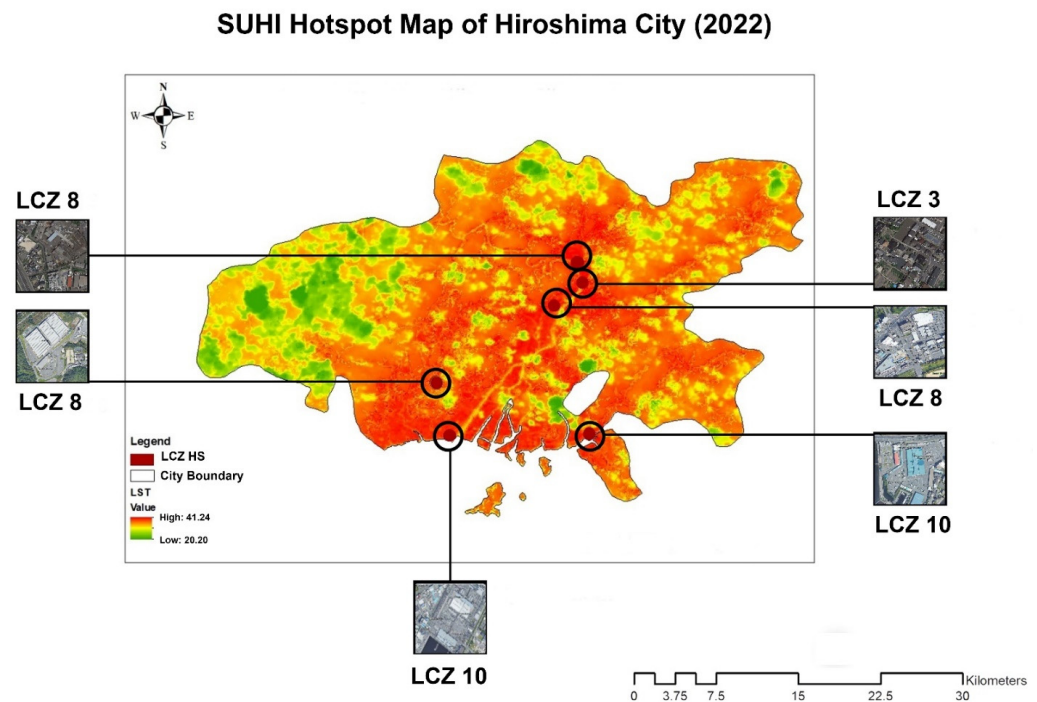


Figure 11. SUHI HS map of Hiroshima city for 2022.

4. Discussion

The findings of this study validate earlier research, including the work of [49], which demonstrates the applicability of the LCZ classification scheme as a standardized frame-

work across diverse macroclimate regions. Despite variations in LST and the SUHI effect among different regions, the LCZ classification scheme remains effective. Furthermore, the contributions of [50] add to the existing body of evidence supporting the utility of LCZs as a valuable tool for examining the impact of urban morphology on regional climate change.

The strong relationship between LCZs and LST is evident in both cities, with only a few LST outliers in LCZ 4. It was demonstrated by [51] that land-cover types have lower LSTs compared to built types, indicating that built areas have higher temperatures. This indicates that both cities' urban morphology is more consistent with the anticipated thermal behavior predicted by the LCZ classification system. This was in line with earlier research [52].

Sapporo City has been able to maintain low levels of the urban heat island effect and had only a 0.5 °C increase in LST, while Hiroshima City experienced a 1.8 °C increase between 2000 and 2022. The difference between Sapporo City's and Hiroshima City's surface temperature increases can be attributed to their different climate classes (Dfa and Cfa, respectively). Sapporo City is classified as having a Dfa climate, which is characterized by lengthy, frigid winters and brief, refreshing summers. This climatic feature aids in reducing the impact of the SUHI effect in the city. Conversely, Hiroshima City is classified as having a Cfa climate, which is distinguished by sweltering and humid summers. This climatic attribute worsens the impact of the SUHI effect in the city.

LST patterns for LCZs were relatively consistent in the two cities over time, despite spatial differences. The temporal analysis of SUHI intensity in Sapporo revealed a pattern of increasing surface temperatures from compact buildings to larger buildings and industrial zones. Additionally, consistent with our own research findings, ref. [53] documented notable SUHI intensity in industrial zones and three compact LCZ classes in two central European cities. On the other hand, large buildings and industrial areas in Hiroshima have always had high SUHI intensity because of their high surface temperatures, which have not changed over time. In line with our findings [50] Additionally, reported that build-up LCZs with heavy industry had the highest surface temperature in Nairobi city, Kenya.

The analysis of UTFVI indicates that Sapporo, categorized as Dfa, exhibited good SUHI thermal comfort overall. However, in Hiroshima City, classified as Cfa, the majority of the study area experienced relatively poor thermal comfort, particularly in large buildings with concrete surfaces and metal roofs, which received the lowest ranking. In line with our own findings, ref. [54] conducted a study on the decadal change of SUHI UTFVI in Tehran city and found a decline in thermal comfort, with a decrease of 59.94% in 2019. Overall, this study confirms that the Dfa class provides significantly better thermal comfort compared to the Cfa class.

The results demonstrate that in both cities, the majority of the SUHI HS and areas with the highest surface temperatures are situated near industrial zones and large low-rise urban forms. Results show that surface temperature locations within LCZ classes in cities are unaffected by Dfa and Cfa climatic classes. Consistent with our findings, a study conducted by [55] determined that the predominant LCZ types in Hong Kong that have the highest UHI intensity are low-rise or mid-rise LCZs. The designated HS will assist planners and decision-makers in thoroughly assessing the thermal effects of various LCZs.

The variation in the intensity of the SUH over time in Sapporo and Hiroshima may be due to differences in the spatial arrangement of built-up and natural environments, which can have an effect on the distribution of land surface temperature in the two cities. For instance, in terms of its urban form, Hiroshima City is more compact than Sapporo City and has more rivers and water bodies, but less vegetation cover. Due to its less compact urban form and greater presence of green spaces, Sapporo city had more LCZs associated with lower LST values, while Hiroshima city had a higher density of LCZs associated with high LST values. Additionally, it implies that the SUHI of the city increases with its compactness. The study found that a compact urban form was associated with an increase in SUHI, taking into account the city's size and aggregation [56].

The study confirms that cities located in warmer climates and with denser urban forms are more susceptible to the SUHI effect. However, further research could explore the impact of green infrastructure on mitigating the SUHI effect in the selected cities.

LCZ 10, LCZ 8, LCZ E, and LCZ 3 are representative of heavy-industry, large low-rise, bare-rock and paved, and compact low-rise areas, respectively. In both the Dfa (Sapporo city) and Cfa (Hiroshima city) climate classifications, these zones have exhibited unfavorable conditions for both the SUHI effect and the UTFVI. The high levels of SUHI and low levels of UTFVI observed in LCZ 10 areas can be attributed to the prevalence of heat-absorbing materials like concrete, asphalt, and metal surfaces. These materials contribute to elevated temperatures and reduced thermal comfort levels for residents in these areas. Similarly, LCZ 8 areas, with large low-rise buildings and commercial activities, also show unpleasant SUHI and UTFVI conditions. These areas have high levels of impervious surfaces, such as roads and parking lots, which increase heat absorption and retention, leading to high temperatures and low thermal comfort levels. LCZ 3 areas, characterized by compact low-rise residential areas, indicate bad SUHI and UTFVI conditions due to the high density of buildings and limited green spaces. This leads to reduced airflow and increased heat retention, resulting in high temperatures and low thermal comfort levels for residents. Interestingly, the differences in climate classification did not impact the SUHI and UTFVI within the LCZ classes. This indicates that the built environment has a more significant impact on the thermal comfort levels of residents than climate classification.

In conclusion, this comparative study of SUHI in two Japanese cities, Sapporo, and Hiroshima, using local-climate-zone classification, highlights the significance of considering the impact of built-up areas on SUHI intensity.

Limitations

Acquiring the USGS's Landsat data for specific months and days proved to be the primary obstacle in this study. Obtaining a cloud-free Landsat image for August was particularly difficult due to heavy rainfall in the two case studies, Sapporo, and Hiroshima. As a result, numerous procedures were required to remove and correct clouds in order to generate the LST maps. Additionally, the Landsat 7 images had scanline errors, which also required multiple correction procedures, presenting another challenge to the research process. Despite these difficulties, the LST maps created provided valuable insights into land surface-temperature patterns and their correlation with LCZs, which can inform future urban planning and climate-change mitigation efforts.

5. Conclusions

Urban areas all over the world have been the subject of in-depth research on the SUHI effect. This study, which compares the spatial variation of LST in two diversely climatic Japanese cities, Sapporo and Hiroshima, over the past 20 years, is no exception. The study looked at how urban morphology and climate conditions affected local climate change using the LCZ classification system.

The utilization of Landsat images spanning 22 years allowed for the derivation of LST, which was then analyzed in conjunction with the LCZ classification scheme. The results reinforced the strong correlation between LCZs and LSTs, with built areas exhibiting higher temperatures compared to other land-cover types. This aligns with previous research showing that urban regions tend to have higher temperatures due to the heat absorption and retention of buildings, roads, and infrastructure.

Significant disparities in the SUHI phenomenon between Sapporo City and Hiroshima City were brought to light by this study. Sapporo City exhibited a negligible alteration in LST, with a mere 0.5-degree Celsius increment observed over the course of the investigation. Conversely, Hiroshima City experienced a more substantial escalation, characterized by an LST augmentation of 1.8 degrees Celsius.

In Sapporo City during the initial phase of the study in 2000, the open low-rise (LCZ 6) registered the highest LST values, followed by the compact mid-rise (LCZ 2) and compact

low-rise (LCZ 3). However, by 2022, a shift in surface temperatures occurred, with heavy industry (LCZ 10) exhibiting the highest LST values, trailed by LCZ 8 (large low-rise) and LCZ 3 (compact low-rise).

Similarly, in Hiroshima City, the LST hierarchy in 2000 portrayed the compact mid-rise (LCZ 2) as the frontrunner, succeeded by heavy industry (LCZ 10) and bare rock and paved surface (LCZ E). However, the LST dynamics underwent modification by 2022, with LCZ 10 emerging as the predominant thermal contributor, followed by bare-rock and paved-surface (LCZ E) and compact low-rise (LCZ 3) aspects.

Particularly striking is the contrasting magnitude of LST alterations, with Hiroshima experiencing more pronounced changes compared to the comparatively moderate shifts observed in Sapporo. These divergent patterns can be attributed to the differing urban morphology of the two cities, with Hiroshima characterized by a more compact urban form and Sapporo exhibiting a less compact arrangement. Additionally, the climatic classifications of Hiroshima (Cfa) and Sapporo (Dfa) contribute to the observed disparities in LST dynamics.

Recent studies have highlighted the association between surface-temperature patterns and the combined effects of urbanization, urban expansion and climate change. However, this observed trend is not applicable to Japanese cities like Hiroshima and Sapporo, with the exception of climate change. This disparity arises from the relatively sluggish pace of urbanization and the absence of urban expansion in these regions. Moreover, the alterations in Local Climate Zone (LCZ) classifications within Hiroshima and Sapporo are minimal and inconspicuous.

Thermal comfort assessment using the widely used UTFVI demonstrated good thermal comfort in Sapporo but relatively poor comfort in Hiroshima. This finding emphasizes the importance of incorporating thermal comfort considerations into urban planning and design to enhance residents' quality of life.

This article emphasizes the substantial impact of the built environment on the SUHI effect and UTFVI within LCZs. LCZ 10, LCZ 8, LCZ E, and LCZ 3 areas in both Dfa and Cfa climate classifications exhibited unfavorable UHI and UTFVI conditions due to factors like a high concentration of heat-absorbing materials, impervious surfaces, and limited green spaces. Interestingly, climate classification did not significantly determine the SUHI and UTFVI patterns within LCZ classes. Hence, urban planning and design interventions should prioritize reducing heat-absorbing materials, increasing green spaces, and promoting airflow in LCZ 10, LCZ 8, LCZ E, and LCZ 3 areas to enhance residents' thermal comfort. These findings hold implications for future urban development in similar zones, emphasizing the need for sustainable urban planning practices that prioritize residents' well-being.

Furthermore, the research revealed that most SUHI hotspots were concentrated near industrial zones, large low-rise areas, paved surfaces, and compact low-rise urban forms. These specific areas may require targeted interventions to reduce the UHI effect and enhance the thermal comfort experienced by residents.

The results of this study carry significant implications for urban planners and decision-makers, providing valuable insights into the thermal effects of different LCZs and strategies to mitigate them. The findings can guide urban planning and design decisions in cities with comparable characteristics, contributing to the creation of more sustainable and livable urban environments.

Considering the results of our paper, we suggest some implications for urban planning:

- The thermal comfort level and hotspots of each LCZ class in the two cities were examined, and it was found that the heavy-industry and large low-rise (LCZ 8, 10, E, and 3) areas were the most vulnerable to the effects of SUHI. This finding suggests that when implementing heat-mitigation measures, urban planners and policymakers should give priority to areas with a heavy industrial presence, and large low-rise, bare-rock and paved, and compact low-rise buildings. Because the SUHI effects in these areas have the potential to seriously harm residents' and employees' health, especially

during heatwaves, they must be addressed. Below are some recommendations for policies that can be put in place to lessen their susceptibility to SUHI:

- In Local Climate Zones 8, 10, E, and 3 there may still be opportunities to increase vegetation cover despite the low-rise structures and heavy industry. In these areas, policies can be put into place to increase the number of trees, green spaces, and green roofs. This might entail giving property owners financial incentives to install green roofs, providing funding for planting trees, and developing new parks and green areas.
- Encouraging the use of sustainable building strategies like green roofs, reflective roofs, and permeable surfaces is important. These design elements can facilitate cooling through evapotranspiration while reducing the amount of heat absorbed by surfaces and buildings.
- Policies can be implemented to increase the reflectivity of surfaces in Local Climate Zones 8, 10, E, and 3. This could include the use of cool pavements, light-colored roofing materials, and reflective coatings.
- Cool roofs reflect more sunlight and absorb less heat than traditional roofs. Policies can be implemented to encourage the use of cool roofs in Local Climate Zones 8, 10, and 3. This could include incentives for property owners to install cool roofs, building codes that require cool roofs for new construction, and educational campaigns to raise awareness of the benefits of cool roofs.
- In Local Climate Zone 10, heavy industry can produce a lot of heat. Policies can be put in place to reduce the impact of these heat sources, such as mandating low-emission machinery for industries, boosting energy efficiency, and encouraging the use of renewable energy sources.

In conclusion, this study offers valuable insights into the SUHI effect and its impact on Sapporo's and Hiroshima's urban areas. It emphasizes the importance of considering climatic conditions and urban morphology when devising mitigation strategies to alleviate the SUHI effect and enhance residents' thermal comfort.

Author Contributions: Conceptualization, N.R. and A.S.; methodology, N.R. and A.S.; software, N.R.; investigation, N.R.; resources, A.S.; data curation, N.R.; writing—original draft preparation, N.R.; writing—review and editing, A.S.; supervision, A.S. All authors have read and agreed to the published version of the manuscript.

Funding: This research received no external funding.

Data Availability Statement: The data used in this study were obtained from USGS Landsat 7 and 8, Google Earth Pro, and the LCZ Generator platform. The Landsat data can be accessed through the USGS Earth Explorer website (<https://earthexplorer.usgs.gov/>), while Google Earth Pro can be downloaded from the Google Earth website (<https://www.google.com/earth/versions/>, 2 March 2023). The LCZ Generator platform can be accessed through the following website (LCZ Generator (rub.de)). Restrictions may apply for accessing and using these datasets, and users are encouraged to consult the relevant terms and conditions. The Landsat satellite dataset is downloaded from the United States Geological Survey (USGS) at (<https://earthexplorer.usgs.gov>) for 2000, 2006, 2011, 2016, and 2022.

Conflicts of Interest: The authors declare no conflict of interest.

References

1. Huang, K.; Li, X.; Liu, X.; Seto, K.C. Projecting global urban land expansion and heat island intensification through 2050. *Environ. Res. Lett.* **2019**, *14*, 114037. [[CrossRef](#)]
2. Yim, S.H.L.; Wang, M.; Gu, Y.; Yang, Y.; Dong, G.; Li, Q. Effect of Urbanization on Ozone and Resultant Health Effects in the Pearl River Delta Region of China. *J. Geophys. Res. Atmos.* **2019**, *124*, 11568–11579. [[CrossRef](#)]
3. Seto, K.C.; Dhakal, S.; Bigio, A.G.; Blanco, H.; Delgado, G.C.; Dewar, D.; Huang, L.; Inaba, A.; Kansal, A.; Lwasa, S.; et al. *Human Settlements, Infrastructure and Spatial Planning*; Cambridge University Press: Cambridge, UK, 2014.
4. Heisler, G.M.; Brazel, A.J. The Urban Physical Environment: Temperature and Urban Heat Islands. In *Urban Ecosystem Ecology*; Wiley: Hoboken, NJ, USA, 2010; pp. 29–56. [[CrossRef](#)]

5. Erdem, U.; Cubukcu, K.M.; Sharifi, A. An analysis of urban form factors driving Urban Heat Island: The case of Izmir. *Environ. Dev. Sustain.* **2021**, *23*, 7835–7859. [[CrossRef](#)]
6. Althor, G.; Watson, J.E.M.; Fuller, R.A. Global mismatch between greenhouse gas emissions and the burden of climate change. *Sci. Rep.* **2016**, *6*, 20281. [[CrossRef](#)]
7. Sharifi, A.; Pathak, M.; Joshi, C.; He, B.-J. A systematic review of the health co-benefits of urban climate change adaptation. *Sust. Cities Soc.* **2021**, *74*, 103190. [[CrossRef](#)]
8. Stemn, E.; Kumi-Boateng, B. Modelling of land surface temperature changes as determinant of urban heat island and risk of heat-related conditions in the Wassa West Mining Area of Ghana. *Model. Earth Syst. Environ.* **2020**, *6*, 1727–1740. [[CrossRef](#)]
9. He, B.-J.; Wang, W.; Sharifi, A.; Liu, X. Progress, knowledge gap and future directions of urban heat mitigation and adaptation research through a bibliometric review of history and evolution. *Energy Build.* **2023**, *287*, 112976. [[CrossRef](#)]
10. Voogt, J.A.; Oke, T.R. Thermal remote sensing of urban climates. *Remote Sens. Environ.* **2003**, *86*, 370–384. [[CrossRef](#)]
11. Venter, Z.S.; Chakraborty, T.; Lee, X. Crowdsourced air temperatures contrast satellite measures of the urban heat island and its mechanisms. *Sci. Adv.* **2021**, *7*, eabb9569. [[CrossRef](#)]
12. Liao, Y.; Shen, X.; Zhou, J.; Ma, J.; Zhang, X.; Tang, W.; Chen, Y.; Ding, L.; Wang, Z. Surface urban heat island detected by all-weather satellite land surface temperature. *Sci. Total Environ.* **2022**, *811*, 151405. [[CrossRef](#)]
13. Avdan, U.; Jovanovska, G. Algorithm for Automated Mapping of Land Surface Temperature Using LANDSAT 8 Satellite Data. *J. Sens.* **2016**, *2016*, 1480307. [[CrossRef](#)]
14. Berger, C.; Rosentreter, J.; Voltersen, M.; Baumgart, C.; Schmuilius, C.; Hese, S. Spatio-temporal analysis of the relationship between 2D/3D urban site characteristics and land surface temperature. *Remote Sens. Environ.* **2017**, *193*, 225–243. [[CrossRef](#)]
15. Gao, Z.; Hou, Y.; Chen, W. Enhanced sensitivity of the urban heat island effect to summer temperatures induced by urban expansion. *Environ. Res. Lett.* **2019**, *14*, 094005. [[CrossRef](#)]
16. Bassani, F.; Garbero, V.; Poggi, D.; Ridolfi, L.; von Hardenberg, J.; Milelli, M. An innovative approach to select urban-rural sites for Urban Heat Island analysis: The case of Turin (Italy). *Urban Clim.* **2022**, *42*, 101099. [[CrossRef](#)]
17. Zhao, Z.; Sharifi, A.; Dong, X.; Shen, L.; He, B.-J. Spatial Variability and Temporal Heterogeneity of Surface Urban Heat Island Patterns and the Suitability of Local Climate Zones for Land Surface Temperature Characterization. *Remote Sens.* **2021**, *13*, 4338. [[CrossRef](#)]
18. Yu, X.; Guo, X.; Wu, Z. Land Surface Temperature Retrieval from Landsat 8 TIRS—Comparison between Radiative Transfer Equation-Based Method, Split Window Algorithm and Single Channel Method. *Remote Sens.* **2014**, *6*, 9829–9852. [[CrossRef](#)]
19. Grover, A.; Singh, R.B. Analysis of Urban Heat Island (UHI) in Relation to Normalized Difference Vegetation Index (NDVI): A Comparative Study of Delhi and Mumbai. *Environments* **2015**, *2*, 125–138. [[CrossRef](#)]
20. Zhang, Y.; Sun, L. Spatial-temporal impacts of urban land use land cover on land surface temperature: Case studies of two Canadian urban areas. *Int. J. Appl. Earth Obs. Geoinf.* **2019**, *75*, 171–181. [[CrossRef](#)]
21. Zhao, C.; Jensen, J.L.R.; Weng, Q.; Currit, N.; Weaver, R. Use of Local Climate Zones to investigate surface urban heat islands in Texas. *GISci. Remote Sens.* **2020**, *57*, 1083–1101. [[CrossRef](#)]
22. Bechtel, B.; Demuzere, M.; Mills, G.; Zhan, W.; Sismanidis, P.; Small, C.; Voogt, J. SUHI analysis using Local Climate Zones—A comparison of 50 cities. *Urban Clim.* **2019**, *28*, 100451. [[CrossRef](#)]
23. Bechtel, B.; Alexander, P.J.; Böhner, J.; Ching, J.; Conrad, O.; Feddema, J.; Mills, G.; See, L.; Stewart, I. Mapping Local Climate Zones for a Worldwide Database of the Form and Function of Cities. *ISPRS Int. J. Geo-Inf.* **2015**, *4*, 199–219. [[CrossRef](#)]
24. Ching, J.; Mills, G.; Bechtel, B.; See, L.; Feddema, J.; Wang, X.; Ren, C.; Brousse, O.; Martilli, A.; Neophytou, M.; et al. WUDAPT: An Urban Weather, Climate, and Environmental Modeling Infrastructure for the Anthropocene. *Bull. Am. Meteorol. Soc.* **2018**, *99*, 1907–1924. [[CrossRef](#)]
25. Stewart, I.D.; Oke, T.R. Local Climate Zones for Urban Temperature Studies. *Bull. Am. Meteorol. Soc.* **2012**, *93*, 1879–1900. [[CrossRef](#)]
26. Nassar, A.K.; Blackburn, G.A.; Whyatt, J.D. Dynamics and controls of urban heat sink and island phenomena in a desert city: Development of a local climate zone scheme using remotely-sensed inputs. *Int. J. Appl. Earth Obs. Geoinf.* **2016**, *51*, 76–90. [[CrossRef](#)]
27. Das, M.; Das, A. Assessing the relationship between local climatic zones (LCZs) and land surface temperature (LST)—A case study of Sriniketan-Santiniketan Planning Area (SSPA), West Bengal, India. *Urban Clim.* **2020**, *32*, 100591. [[CrossRef](#)]
28. Shi, Y.R.; Xiang, Y.R.; Zhang, Y.F. Urban Design Factors Influencing Surface Urban Heat Island in the High-Density City of Guangzhou Based on the Local Climate Zone. *Sensors* **2019**, *19*, 3459. [[CrossRef](#)]
29. Yasushi, S.; Goshin, N. The Relationship between Urban Surface Indices and Heat Islands in High and Low Building Areas. *Geogr. Rev. Jpn. Ser. B* **2010**, *82*, 196–204. [[CrossRef](#)]
30. Zhou, X.; Okaze, T.; Ren, C.; Cai, M.; Ishida, Y.; Mochida, A. Mapping local climate zones for a Japanese large city by an extended workflow of WUDAPT Level 0 method. *Urban Clim.* **2020**, *33*, 100660. [[CrossRef](#)]
31. Mutani, G.; Todeschi, V.; Matsuo, K. Urban Heat Island Mitigation: A GIS-based Model for Hiroshima. *Instrum. Mes. Métrologie* **2019**, *18*, 323–335. [[CrossRef](#)]
32. Ignatius, M.; Xu, R.; Hou, Y.; Liang, X.; Zhao, T.; Chen, S.; Wong, N.H.; Biljecki, F. Local climate zones: Lessons from singapore and potential improvement with street view imagery. *ISPRS Ann. Photogramm. Remote Sens. Spat. Inf. Sci.* **2022**, *10*, 121–128. [[CrossRef](#)]

33. Wang, R.; Ren, C.; Xu, Y.; Lau, K.K.-L.; Shi, Y. Mapping the local climate zones of urban areas by GIS-based and WUDAPT methods: A case study of Hong Kong. *Urban Clim.* **2018**, *24*, 567–576. [CrossRef]
34. Cai, M.; Ren, C.; Xu, Y.; Lau, K.; Wang, R. Investigating the relationship between local climate zone and land surface temperature using an improved WUDAPT methodology—A case study of Yangtze River Delta, China. *Urban Clim.* **2017**, *24*, 485–502. [CrossRef]
35. Kim, H.-J.; Wang, B.; Ding, Q.; Chung, I.-U. Changes in Arid Climate over North China Detected by the Köppen Climate Classification. *J. Meteorol. Soc. Japan Ser. II* **2008**, *86*, 981–990. [CrossRef]
36. Szabó, A.I.; Ács, F.; Breuer, H. Larger Carpathian region climate according to Köppen, Feddema and the Worldwide Bioclimatic Classification System methods. *Int. J. Climatol.* **2021**, *41*, E2482–E2496. [CrossRef]
37. Peel, M.C.; Finlayson, B.L.; McMahon, T.A. Updated world map of the Köppen-Geiger climate classification. *Hydrol. Earth Syst. Sci.* **2007**, *11*, 1633–1644. [CrossRef]
38. Brozovsky, J.A.; Gaitani, N.; Gustavsen, A. A systematic review of urban climate research in cold and polar climate regions. *Renew. Sustain. Energy Rev.* **2020**, *138*, 110551. [CrossRef]
39. Macrotrends. Macrotrends Website. Available online: <https://www.macrotrends.net/cities/204581/sapporo/population/> (accessed on 7 April 2023).
40. COH. The City of Hiroshima (COF) Official Website. Available online: <https://www.city.hiroshima.lg.jp/site/english/> (accessed on 7 April 2023).
41. Solanky, V.; Singh, S.; Katiyar, S. *Land Surface Temperature Estimation Using Remote Sensing Data*; Springer: Singapore, 2018; pp. 343–351. [CrossRef]
42. Hashimoto, S.; Sato, T. Estimation method of systematic uncertainties in Monte Carlo particle transport simulation based on analysis of variance. *J. Nucl. Sci. Technol.* **2019**, *56*, 345–354. [CrossRef]
43. Rodler, A.; Leduc, T. Local climate zone approach on local and micro scales: Dividing the urban open space. *Urban Clim.* **2019**, *28*, 100457. [CrossRef]
44. Xia, H.P.; Chen, Y.H.; Song, C.H.; Li, J.X.; Quan, J.L.; Zhou, G.M. Analysis of surface urban heat islands based on local climate zones via spatiotemporally enhanced land surface temperature. *Remote Sens. Environ.* **2022**, *273*, 153–224. [CrossRef]
45. Yong, Z.; Tao, Y.; Xingfa, G.; Yu-xiang, Z.; Shan-shan, Y.; Wen-jun, Z.; Xiaowen, L. Land Surface Temperature Retrieval from CBERS-02 IRMSS Thermal Infrared Data and Its Applications in Quantitative Analysis of Urban Heat Island Effect. *J. Remote Sens.* **2006**, *10*, 789.
46. Hidalgo-García, D.; Arco-Díaz, J. Modeling the Surface Urban Heat Island (SUHI) to study of its relationship with variations in the thermal field and with the indices of land use in the metropolitan area of Granada (Spain). *Sustain. Cities Soc.* **2022**, *87*, 104166. [CrossRef]
47. Nautiyal, G.; Maithani, S.; Sharma, A. Exploring the Relationship Between Spatio-temporal Land Cover Dynamics and Surface Temperature Over Dehradun Urban Agglomeration, India. *J. Indian Soc. Remote Sens.* **2021**, *49*, 1307–1318. [CrossRef]
48. Cardoso, R.d.S.; Amorim, M.C.d.C.T. Urban heat island analysis using the ‘local climate zone’ scheme in Presidente Prudente, Brazil. *Investig. Geográficas* **2018**, *69*, 107–118. [CrossRef]
49. Eldesoky, A.H.M.; Gil, J.; Pont, M.B. The suitability of the urban local climate zone classification scheme for surface temperature studies in distinct macroclimate regions. *Urban Clim.* **2021**, *37*, 100823. [CrossRef]
50. Ochola, E.M.; Fakharizadehshirazi, E.; Adimo, A.O.; Mukundi, J.B.; Wesonga, J.M.; Sodoudi, S. Inter-local climate zone differentiation of land surface temperatures for Management of Urban Heat in Nairobi City, Kenya. *Urban Clim.* **2020**, *31*, 100540. [CrossRef]
51. Unal Cilek, M.; Cilek, A. Analyses of land surface temperature (LST) variability among local climate zones (LCZs) comparing Landsat-8 and ENVI-met model data. *Sustain. Cities Soc.* **2021**, *69*, 102877. [CrossRef]
52. Gholami Rostam, M.; Beck, C. Towards the determination of driving factors of varying LST-LCZ relationships: A case study over 25 cities. *Geogr. Pannonica* **2019**, *23*, 289–307. [CrossRef]
53. Geletič, J.; Lehnert, M.; Dobrovolný, P. Land Surface Temperature Differences within Local Climate Zones, Based on Two Central European Cities. *Remote Sens.* **2016**, *8*, 788. [CrossRef]
54. Najafzadeh, F.; Mohammadzadeh, A.; Ghorbanian, A.; Jamali, S. Spatial and Temporal Analysis of Surface Urban Heat Island and Thermal Comfort Using Landsat Satellite Images between 1989 and 2019: A Case Study in Tehran. *Remote Sens.* **2021**, *13*, 4469. [CrossRef]
55. Zheng, Y.; Ren, C.; Shi, Y.; Yim, S.H.L.; Lai, D.Y.F.; Xu, Y.; Fang, C.; Li, W. Mapping the spatial distribution of nocturnal urban heat island based on Local Climate Zone framework. *Build. Environ.* **2023**, *234*, 110197. [CrossRef]
56. Kang, S.; Lee, D.; Park, J.; Jung, J. Exploring Urban Forms Vulnerable to Urban Heat Islands: A Multiscale Analysis. *Sustainability* **2022**, *14*, 3603. [CrossRef]

Disclaimer/Publisher’s Note: The statements, opinions and data contained in all publications are solely those of the individual author(s) and contributor(s) and not of MDPI and/or the editor(s). MDPI and/or the editor(s) disclaim responsibility for any injury to people or property resulting from any ideas, methods, instructions or products referred to in the content.